Whitmarsh, R.B., Sawyer, D.S., Klaus, A., and Masson, D.G. (Eds.), 1996
Proceedings of the Ocean Drilling Program, Scientific Results, Vol. 149

18. IN SITU VELOCITIES OF SEDIMENTARY ROCKS FROM THE IBERIA ABYSSAL PLAIN[1]

Dennis L. Harry[2] and Mike Batzle[3]

ABSTRACT

The acoustic properties of deep-sea claystones and silty claystones recovered on Ocean Drilling Program Leg 149 were examined under pressure conditions at and above the expected in situ effective pressure in order to estimate acoustic velocity in the upper few hundred meters below seafloor (mbsf) on the Iberia Abyssal Plain. In situ effective pressure and velocity for each of the samples studied is indicated by an inflection point on the measured velocity vs. pressure curve. The estimated in situ velocities range from 1995 to 2470 m s^{-1} for sediments buried from 120 to 510 mbsf, and the estimated in situ effective pressure ranges from 2.2 to 6.5 MPa. Velocities estimated from the laboratory study are similar to those determined from marine seismic-refraction surveys. The laboratory data suggest a velocity gradient of about 0.63 m s^{-1} at depths shallower than 320 mbsf and a velocity gradient of 4.4 m s^{-1}/m between 335 and 370 mbsf. The steep velocity gradient in the interval between 335 and 370 mbsf may be responsible for a strong refraction observed on marine seismic data at a depth of a few hundred meters. The in situ effective pressure increases abruptly below about 200 mbsf. This may reflect a change from poorly consolidated sediments above 200 mbsf to consolidated sediments below 200 mbsf.

In situ pressure estimates combined with shipboard grain-density measurements provide an estimate of the porosity and density of the upper few hundred meters of sediment beneath the Iberia Abyssal Plain. The estimated porosity shows wide scatter, but generally appears to follow an exponential decrease in porosity with depth. Density generally appears to increase linearly with depth in the upper 600 mbsf according to the relation $\rho(z) = 1.7945 + 0.001\ z$, where z is depth below seafloor (in meters) and ρ is density in grams per cubic centimeter.

INTRODUCTION

Sediments recovered during Leg 149 provide unique constraints on the acoustic properties of the first few hundred meters of strata beneath the seafloor on the Iberia Abyssal Plain. This interval is dominantly claystone, silty claystone, clayey siltstone, and nannofossil claystone (Sawyer, Whitmarsh, Klaus, et al., 1994). The sediments were deposited largely by turbidity flows with intervening periods of pelagic and hemipelagic sedimentation during the early Pliocene to the middle Miocene. Some of the sedimentary sequence shows evidence of contourite reworking. Because of the lack of drilling activity on the margin, no direct constraints are available on the acoustic properties of these sediments. In order to alleviate this problem, compressional-wave velocity measurements were conducted aboard ship during the Leg 149 cruise. A fundamental difficulty with the shipboard velocity measurements is that they were conducted at atmospheric pressure. Because velocity is strongly dependent upon pressure, the shipboard measurements are poor indicators of the in situ velocity (Hamilton, 1971). Not surprisingly, the shipboard velocity measurements are inconsistent with velocities estimated from seismic refraction and reflection studies (e.g., Whitmarsh et al., 1990). The seismic data generally indicated compressional velocities of 1.84 to 2.6 km s^{-1} in the cored interval, whereas the shipboard measurements consistently indicated velocities less than 1.8 km s^{-1}. The most likely cause of the discrepancy between the shipboard and seismic measurements is decompaction of the samples following their recovery from the subseafloor. Decompaction results in an increase in porosity and may be accompanied by release of gaseous phases into the pore fluid. Both factors contribute to a reduction in acoustic velocity (Hamilton, 1971; Boyce, 1973; Stoll, 1977). In order to test this hypothesis and to better estimate the in situ acoustic properties of the sediments on the Iberia Abyssal Plain, an experimental study was undertaken to measure compressional- and shear-wave velocities in samples recovered during Leg 149 at pressure conditions comparable to the in situ pressure. Only the compressional-wave data are discussed here. Because problems with hole stability prevented collection of acoustic logs in most of the drill holes, no other direct measure of in situ velocity is available. Because velocity depends strongly on porosity, density, and the degree of consolidation, the study also provides indirect constraints on these properties in situ.

EXPERIMENTAL TECHNIQUE

The shore-based study focused on samples taken from lithostratigraphic Units I and II at Sites 897, 898, 899, and 900. These sediments range in age from early Pliocene to middle Miocene and were deposited well after the cessation of rifting. The environment of deposition is inferred to be off-shelf deep water, allowing for the predominance of turbidite and contourite deposits (Sawyer, Whitmarsh, Klaus, et al., 1994). Figure 1 shows the results of the shipboard velocity measurements over the interval encompassing these lithostratigraphic units. Shown for comparison is a velocity profile derived from a marine seismic refraction study reported by Whitmarsh et al. (1990). The shipboard velocity measurements clearly underestimate the in situ velocity for most samples.

The basic approach used to infer the in situ acoustic velocity is to place the sample under pressure conditions thought to be similar to the in situ pressure and measure the traveltime of an electrically generated acoustic pulse through the sample. The pulse generator produces a 350-V square wave with a pulse width of 2 µs, which is repeated at a frequency of 400 kHz. The electrical pulse is converted into an acoustic signal by means of a piezoelectric transducer, which is placed adjacent to one end of the sample (Fig. 2). A transducer on

[1]Whitmarsh, R.B., Sawyer, D.S., Klaus, A., and Masson, D.G. (Eds.), 1996. *Proc. ODP, Sci. Results,* 149: College Station, TX (Ocean Drilling Program).
[2]Department of Geology, The University of Alabama, Box 870338, Tuscaloosa, AL 35487, U.S.A. dharry@geophys.geo.ua.edu
[3]Geophysics Department and Institute for Resource and Environmental Geosciences, Colorado School of Mines, Golden, CO 80401, U.S.A.

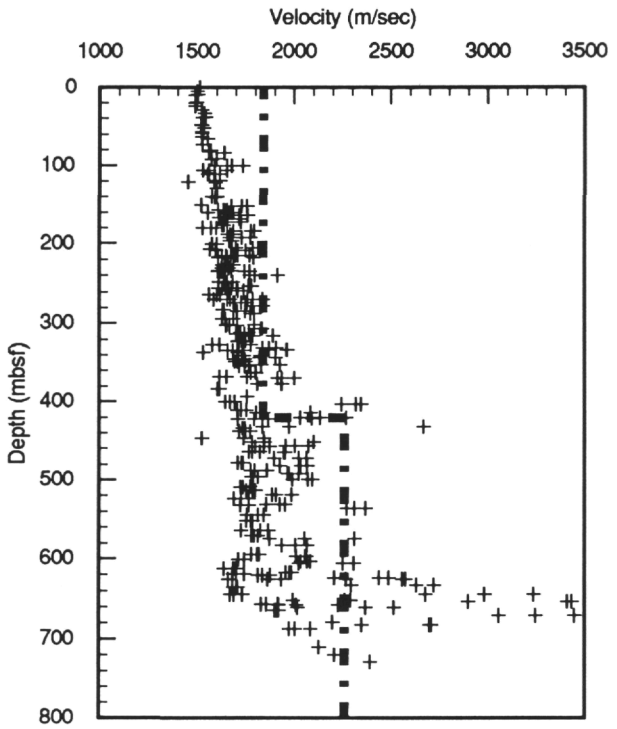

Figure 1. Shipboard velocity measurements at Sites 897, 898, 899, and 900 (plus symbols). The dashed line indicates the results from sonobuoy Line 1 reported by Whitmarsh et al. (1990). The high velocities between 620 and 670 mbsf are from lithified samples in lithostratigraphic Subunit IIIB and Unit IV at the top of the basement high beneath Site 897.

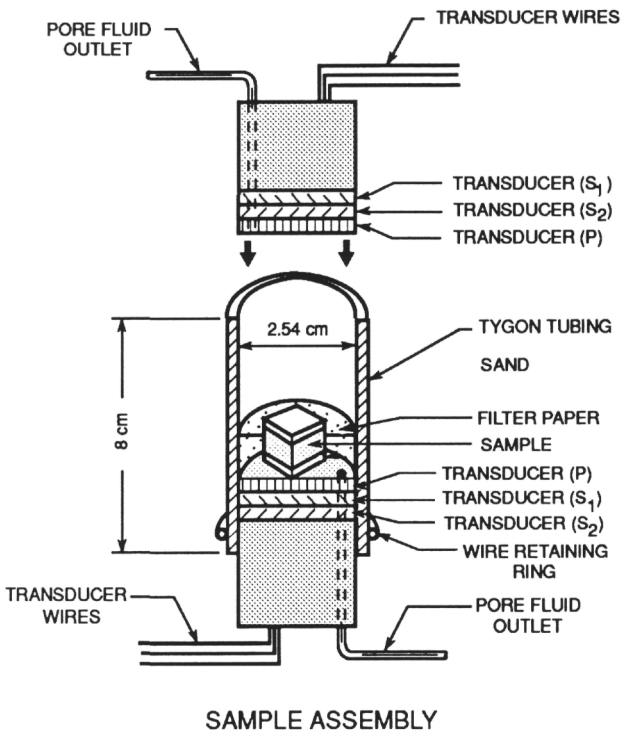

Figure 2. Sample assembly. The sample is wrapped in filter paper and encased in a tygon tube. Sand is packed into the tube to fill the space between the sample and the tube wall, allowing circulation of pore fluid through the sample. A stacked series of transducers (compressional wave, P, and two orthogonal shear waves, S_1 and S_2) is placed on either end of the tube, which is clamped with a wire retaining ring. A pore-fluid outlet through the transducers is positioned in contact with the sand pack.

the other end of the sample detects the pulse and converts it into an electrical signal, which is recorded by a digital oscilloscope. Velocity is calculated by dividing the sample length by the traveltime of the pulse (after correcting the observed traveltime for the time required for the pulse to traverse the transducers). A series of three transducers were stacked in order to record the compressional wave and shear waves with particle displacement in two orthogonal directions (Fig. 2). The direction of wave propagation was perpendicular to bedding (vertical). The shipboard velocity measurements indicated significant anisotropy (typical about 5%) in the samples, with the horizontal directions of wave propagation being faster than the vertical direction. The laboratory data presented here thus represent the slow direction of wave propagation and may not be directly comparable to velocities determined from seismic reflection and sonobuoy experiments because raypaths in these experiments have both horizontal and vertical components.

The experimental apparatus is shown schematically in Figure 3. The sample/transducer package is placed inside a pressure vessel filled with hydraulic fluid. The confining pressure and the pore pressure in the sample are independently controlled by separate pump systems. In order to isolate the sample from the confining fluid, the sample was encased in a tygon tube that was clamped at the ends with a wire retaining ring (Fig. 2). Samples were trimmed to rectangular prisms (approximately 1.2 × 0.8 × 0.8 cm) and wrapped in filter paper before placing them in the tygon tube. Sand was packed around the sample to fill the tube, and the transducer assembly was positioned so that the pore fluid outlet was in contact with the sand. This allowed circulation of pore fluid through the sample while preventing the sample from extruding into the pore-fluid outlet at high pressure.

The change in velocity with pressure in sediments results from compaction, so it is necessary to estimate the amount of shortening in the sample at high pressure. It was not possible to directly measure sample strain during the velocity studies. Instead, the length of the sample was measured before and after the experiment. The observed shortening was assumed to be the maximum amount of shortening the sample underwent (i.e., at the highest pressure). The length of the sample at intermediate pressures was determined by linearly interpolating between the length at atmospheric pressure (measured prior to the experiment) and the inferred length at maximum pressure (measured after the experiment). This approach assumes that compaction depends linearly on pressure and that no rebound or decompaction of the sample occurred prior to removing it from the pressure vessel. The validity of these assumptions is discussed in the next section, where the traveltime and velocity data are presented.

In porous, unconsolidated sediments, compaction (and hence velocity) is dependent mostly upon the effective pressure,

$$P_e = P_c - P_p, \quad (1)$$

where P_c is the confining pressure and P_p is the pore pressure (Stoll, 1977; Das, 1983). Because the in situ pore pressure is not known, traveltime measurements were made at a range of effective pressures up to 99 MPa. Two series of experiments were conducted on each sample. First, undrained tests were conducted with the sample saturated with salt water (salinity 30,000 ppm) and pore pressure held equal to half the confining pressure. Measurements were taken at several stages as the confining pressure was raised from atmospheric pressure to the maximum confining pressure, and again as the confining pressure was lowered. Second, drained tests were then conducted with the pore-fluid outlet vented to atmospheric pressure, as the confining pressure was again raised to a maximum and decreased back

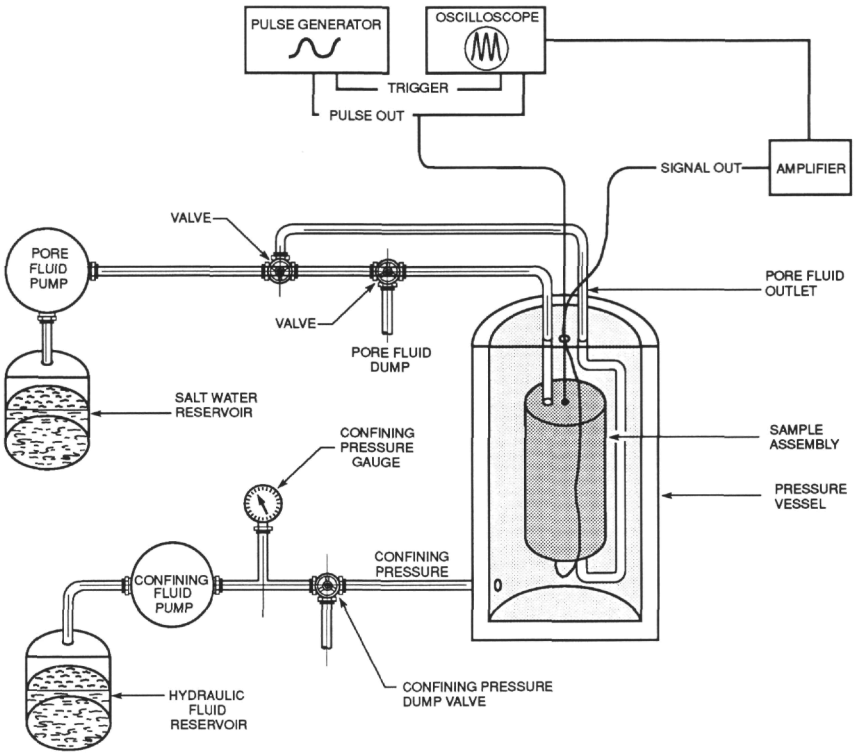

Figure 3. Schematic illustration of the experimental apparatus. The sample assembly is placed in a pressure vessel filled with hydraulic fluid. An acoustic wave is generated by sending an electronic pulse through the upper transducer, which is detected by the lower transducer and recorded with a digital oscilloscope.

Table 1. Samples used in velocity studies.

Core, section	Unit	Lithology	Burial (mbsf)	Water depth (m)	Shipboard velocity (m/s)
149-897C-					
34R-1	IIC	Silty claystone	369	5315	1617
48R-5	IIC	Silty claystone	510	5315	1779
149-898A-					
13H-5	I	Silty clay	120	5279	1559
20X-3	IIB	Silty claystone	181	5279	1530
149-899B-					
1R-2	IIB	Claystone with silt	232	5291	1628
12R-4	IIB	Silty claystone	336	5291	1738
149-900A-					
35R-2	IIB	Claystone	317	5045	1834

to atmospheric pressure. To minimize the bias introduced by time-dependent compaction and pore-fluid movement, the samples were held at each pressure for periods of 20 to 45 min before the traveltime measurements were made. This period of time was deemed sufficient by observing the traveltime periodically while the sample was equilibrating. Most samples ceased to show a change in traveltime after 15-20 min. This was verified by allowing three of the samples to equilibrate at high pressure for 10 hr; no change was observed in the traveltime between measurements taken after 20 min and measurements taken after 10 hr. All experiments were conducted at room temperature, which varied between 20° and 23 °C.

Experimental Problems

A major problem with the experimental technique was that coupling between the transducers and the sample was inadequate to generate a detectable acoustic wave until the effective pressure had been raised to ~2-5 MPa. Because the bulk density of most of the samples is about 1.9 g/cc (Sawyer, Whitmarsh, Klaus, et al., 1994) and the depth of burial ranged from 120 to 510 meters below seafloor (mbsf), the first measurement was generally at or above the expected in situ lithostatic pressure. Velocities at lower pressures were interpolated by using the shipboard measurement of the velocity at atmospheric pressure. Little seismic energy propagated through the poorly consolidated sand packed around the samples except at very high effective pressures. At effective pressures above ~25 MPa, a second arrival—attributed to ray travel through the sand pack—was detected in some experiments. However, in all instances this arrival was sufficiently slow to be clearly separated from the arrival that represented ray travel through the sample.

Another problem with the shore-based study is that the samples subjected to testing under pressure do not completely represent all of the lithologies recovered during Leg 149. In general, clays and silty clays from lithostratigraphic Unit II were found to be coherent enough to withstand testing under pressure, and these sediments suffered little observable post-cruise deterioration. Predominantly silty samples were not coherent enough to withstand testing under pressure. Chalk and calcareous clay samples were found to have undergone irreparable deterioration (drying and cracking) during the period between recovery and post-cruise testing. Analyses of several nannofossil clay samples were attempted, but all but one of these samples underwent significant deformation during testing and the results were deemed unreliable.

Finally, in some runs, the pore-fluid outlet became obstructed, preventing expulsion of pore fluid. As a result, pore pressures in some experiments were higher than intended, and the effective pressure was lower than recorded. This difficulty is easily recognized in the data, and generally was rectified during the experiment so that at least part of the data collected in these experiments is deemed accurate. Problems with pore pressure are discussed below for those experiments in which this problem was encountered.

Sample Description

Samples were selected from those used for shipboard acoustic velocity measurements, and they generally represent the dominant lithologies in Leg 149 cores. As discussed above, however, lithologies that do not have a high clay content were not coherent enough

Table 2. Measured traveltimes and *P*-wave velocities estimated from laboratory data.

Core, section	Length* (cm)		Pressure (MPa)			Traveltime (m/s)	Velocity** (m/s)	
	Initial	Final	P_c	P_p	P_e	Δt_p	Uncorrected	Corrected
149-897C-								
34R-1	1.45	1.25	5	2	3	9.34	1918	1908
			10	4	5	8.18	2268	2246
			20	10	10	7.62	2486	2442
			49	24	26	6.36	3174	3025
			68	33	35	6.04	3414	3198
			100	49	50	5.70	3712	3369
			50	24	27	6.18	3304	3144
			10	4	6	6.78	2906	2873
			11	0	11	6.74	2929	2873
			50	0	50	5.84	3583	3254
			75	0	75	5.60	3810	3287
			50	0	50	5.82	3601	3270
			10	0	10	6.60	3015	2960
48R-5	1.33	1.28	5	2	3	7.94	2174	2170
			10	4	6	7.38	2392	2385
			20	10	10	6.88	2628	2614
			49	24	26	6.22	3021	2979
			68	28	40	5.74	3390	3317
			99	49	50	5.52	3591	3493
			50	24	27	5.84	3306	3258
			11	4	6	6.56	2805	2795
			10	0	10	6.56	2805	2790
			50	0	50	5.88	3273	3185
			74	0	74	5.52	3591	3447
			50	0	50	5.78	3356	3265
			10	0	10	6.44	2878	2862
149-898A-								
13H-5	2.11	1.92	4	2	2	12.80	1920	1912
			10	5	6	11.15	2259	2235
			20	9	11	10.94	2311	2263
			46	24	22	10.66	2384	2282
			100	50	50	10.06	2557	2306
			52	24	28	10.58	2406	2274
			12	5	8	11.52	2173	2141
			10	0	10	10.78	2352	2308
			19	0	19	9.86	2621	2523
			51	0	51	8.42	3191	2875
			73	0	73	7.96	3430	2939
			98	0	98	7.58	3656	2956
			52	0	52	8.02	3397	3050
			12	0	12	9.38	2787	2721
20X-3	2.05	1.98	4	2	2	12.06	1997	1995
			10	5	5	11.82	2044	2040
			20	10	9	11.06	2212	2203
			50	25	25	9.34	2717	2687
			20	10	10	10.08	2474	2463
			11	5	6	10.56	2339	2332
			10	0	10	10.22	2433	2422
			20	0	20	9.72	2587	2564
			50	0	50	8.44	3086	3017
			75	0	75	8.06	3274	3164
149-899B-								
1R-2	2.52	2.07	12	6	6	12.01	2469	2413
			23	12	11	11.01	2737	2619
			49	25	24	9.77	3166	2868
			74	37	37	8.89	3559	3041
			92	46	46	8.59	3712	3050
			50	25	25	9.28	3372	3047
			12	6	6	10.16	3016	2944
			12	0	12	10.35	2949	2806
12R-4†	2.95	2.82	0	0	0	19.24	1689	1689
			7	0	7	16.02	2071	2059
			12	0	12	14.94	2241	2217
			22	0	22	13.18	2588	2536
			50	0	50	11.43	3059	2921
			73	0	73	10.94	3223	3009
			99	0	99	10.45	3406	3099
			12	0	12	12.60	2727	2697
			13	7	6	12.50	2753	2737
			25	12	12	12.01	2885	2852
			50	25	25	11.43	3059	2989
			96	50	45	10.55	3367	3228
			51	25	26	10.55	3367	3288
			25	12	13	11.13	3157	3121
			12	6	6	11.62	3000	2984
149-900A-								
35R-2	1.54	1.44	4	2	2	9.70	1956	1951
			10	4	6	9.34	2050	2034
			20	10	10	8.66	2253	2223
			49	24	25	7.52	2703	2613
			96	49	47	6.68	3169	2969
			51	24	27	7.30	2811	2708
			10	5	6	7.88	2543	2524
			10	0	10	7.74	2603	2567
			20	0	20	7.52	2703	2630

Table 2 (continued).

Core, section	Length* (cm)		Pressure (MPa)			Traveltime (m/s)	Velocity** (m/s)	
	Initial	Final	P_c	P_p	P_e	Δt_p	Uncorrected	Corrected
			48	0	48	6.68	3169	2962
			74	0	74	6.44	3333	2998
			51	0	51	6.66	3182	2964
			12	0	12	7.54	2693	2649

Notes: * = length was measured before and after the experiment; ** = corrected velocity is estimated by interpolating the change in sample length during the experiment (see text); P_c = confining pressure; P_p = pore pressure; $P_e = P_c - P_p$ = effective pressure; † = the drained test was conducted before the undrained test for Section 149-899B-12R-4.

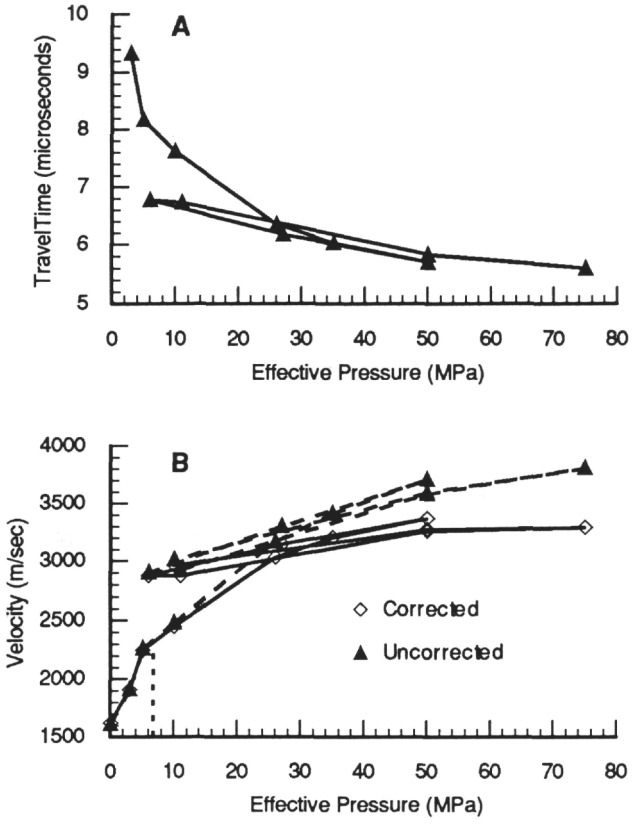

Figure 4. **A.** Traveltimes for Section 149-897C-34R-1. **B.** Velocity curve for Sample 149-897C-34R-1. The uncorrected velocity curve does not account for sample shortening during the experiment. The corrected curve is based on a sample length determined by linearly interpolating between the length of the sample at atmospheric pressure (measured before the experiment) and the maximum pressure (taken to be the sample length after the experiment). The vertical dashed line indicates the best estimate of the in situ effective pressure. See text for discussion.

for testing. The silty clays to clayey silts examined in this research typically represent more than 60% of the core section from which the samples were taken. In addition, core recovery probably was not entirely representative of the lithologies encountered during drilling because non-cohesive lithologies are difficult to recover. Of the sufficiently coherent lithologies, 13 samples were selected that showed minimal signs of post-recovery deterioration (i.e., no obvious drying or cracking of samples). Deterioration was minimized by placing the samples in sealed containers immediately after the shipboard measurements were conducted. Six of the samples showed obvious signs of deformation after the experiment, and the results of those tests are not discussed here. The remaining seven samples are listed in Table 1, with sample names corresponding to the hole, core, and section from which they were taken.

RESULTS

Velocity Measurements

The experimental results are given in Table 2. Figure 4 shows the results for Section 149-897C-34R-1, which is a typical example. During the undrained test, the traveltime initially decreases sharply with increasing effective pressure (Fig. 4A). This is typical behavior for a poorly consolidated sediment undergoing compaction at pressures below the maximum pressure to which it has been previously subjected. The rapid decrease in traveltime is attributed to compaction of the sample arising from collapse of pore space, which developed during decompaction of the sample following recovery (see discussions by Tschebotarioff, 1952; Lambe and Whitman, 1969; Das, 1983). The traveltime continues to decrease above 4.5 MPa, but at a decreasing gradient. This is interpreted as compaction at pressures greater than the highest pressure the sample has previously experienced. Post-recovery pore space has largely collapsed, and continued compaction requires grain re-arrangement and pore-fluid expulsion (Lambe and Whitman, 1969). The point of maximum curvature in the traveltime vs. pressure curve indicates the maximum pressure that the sample has previously experienced. This must occur somewhere between the second and third data points (at 5 MPa and 10 MPa, respectively) in this experiment, so the effective pressure is taken to be 7.5 MPa ± 2.5 MPa. Assuming no great thickness of sediment has been eroded from the overlying strata, this is the in situ effective pressure P_e'. Above 26 MPa, the traveltime curve becomes nearly linear. This is interpreted to indicate nearly complete closure of post-recovery pore space. Further compaction requires fracture and reorientation of the sample grains (e.g., Lambe and Whitman, 1969; Das, 1983). Following the measurement at 50 MPa, the confining pressure and pore pressure were reduced incrementally until the effective pressure reached 6 MPa. The traveltime increases during this sequence of measurements, but only slightly (see the lower traveltime leg in Fig. 4A). This "hysteresis curve" is typical of sediments, and it indicates that the sample has been compressed beyond its most compact previous state during the experiment, resulting in irreversible grain rearrangement (Das, 1983). The measurement taken at an effective pressure of 6 MPa had a confining pressure of 10 MPa and a pore pressure of 4 MPa. After this measurement was taken the pore pressure was released, allowing the effective pressure to rise to 11 MPa (equal to the confining pressure). The drained test was then conducted at confining pressures up to 75 MPa. The traveltimes during this sequence of measurements were generally close to those obtained during the undrained test, indicating that velocity changes are mostly due to changes in the effective pressure, as expected.

The variation of velocity with pressure for Section 149-897C-34R-1 is shown in Figure 4B. The "uncorrected" curve is the velocity calculated by assuming that no shortening of the sample occurred during the experiment. The "corrected" curve is determined by interpolating for the length of the sample at the pressure at each measurement point as discussed previously. The corrected curve shows no increase in velocity above 50 MPa, suggesting that this sample underwent little rebound as the pressure was lowered. If it had undergone rebound, the length of the sample at the highest pressure would be

less than the length measured after the experiment, and the true velocity at high pressure would be less than that shown in Figure 4B. This would require the velocity curve to decrease at high pressure. This is unlikely, so it is inferred that the length of the sample measured after the experiment represents the sample length at high pressure.

The velocity curve mimics the traveltime curve, showing a dramatic increase in velocity with increasing pressure below P_e', maximum curvature at P_e', and a decrease in slope above P_e'. The velocity at P_e' is the expected in situ velocity, and it is picked as the intersection of straight lines fitting the high-pressure and low-pressure portions of the velocity curve. The nearly flat velocity curve above ~25 MPa suggests that the lithology represented by Section 149-897C-34R-1 will have a maximum velocity of not much greater than 3375 m s^{-1} at depths where the effective pressure is greater than 25 MPa. This velocity is similar to that determined for deeper portions of the sedimentary sequence on the Iberia Abyssal Plain determined from refraction surveys (Whitmarsh et al., 1990).

The corrected velocity curves for the other samples are shown in Figure 5. Not all of the samples have velocity curves with P_e' and V_{max} as clearly defined as in Section 149-897C-34R-1. For example, Section 149-898A-20X-3 continues to show a moderate increase in velocity at high pressure and the point of maximum curvature is less obvious (Fig. 5C). In this case, P_e' has relatively large error bars associated with it. The continued increase in velocity at high pressure may indicate either that:

1. the sediment is more compressible at high pressure;
2. the sample had abnormally high in situ pore pressure, so significant porosity and permeability existed. As a result, consolidation and the associated steep velocity increase continues at pressures above the highest pressure previously experienced; or
3. the sample underwent some rebound before it was removed from the pressure vessel, and so the velocity at high pressure is overestimated. It is not possible to differentiate between these three possibilities with the available data, so V_{max} is poorly constrained.

Several experimental problems that are worth further comment are evident in the curves in Figure 5. For Section 149-898A-13H-5 (Fig. 5B) the low-velocity leg of the curve indicates measurements taken during the undrained test. The high-velocity leg of the curve indicates measurements taken during the drained test. It was discovered after the undrained experiment that the pore-pressure outlet had become clogged by clay, preventing expulsion of pore fluid from the sample during the latter stages of the undrained experiment. As a result, pore pressures were high, and the effective pressure on the low-velocity leg was much lower than indicated on the figure. The low-velocity leg of Figure 5B is erroneous and should not be considered. The pore-fluid outlet was cleared before running the drained test (high-velocity leg), so the high-velocity leg of the curve is considered accurate. On Section 149-899B-1R-2 (Fig. 5D), a leak in the hydraulic-fluid reservoir developed before measurement of the last data point (P = 12 MPa, V = 2721 m s^{-1}). The last data point is erroneous, and the experiment was terminated after this measurement (as a result, there is no undrained series of measurements on this sample).

Estimated In Situ Velocity and Pressure

The estimated in situ velocities and effective pressures determined from Figure 5 are given in Table 3. The in situ velocity generally increases monotonically with increasing effective pressure, consistent with a decrease in porosity and increasing sediment compaction during burial. Plotted as a function of depth, the estimated P_e' and velocity data show a reasonably uniform trend between all four sites (Fig. 6). Note that the estimated velocity for Section 149-899B-1R-2 at 232 mbsf falls off the trend of the other data and has large error bars associated with it. This data point is considered suspect because poor transducer/sample coupling prevented measurement of the velocity at low pressures. The first data point obtained for this sample was at an effective pressure of 6 MPa, much higher than the lithostatic pressure at this depth. The uniform trend in velocity as a function of depth for the other samples is not surprising for Sites 897, 898, and 899. The shipboard velocity measurements showed a consistent linear increase in velocity with depth of burial in the sediments, with a similar slope observed in data from all three sites (Fig. 1; Sawyer, Whitmarsh, Klaus, et al., 1994). Two aspects of the data shown in Figure 6 were unanticipated, however. First, the data point for Site 900 falls within the trend of the data from the other three sites. The shipboard velocity measurements for Site 900 show a markedly different slope when plotted as a function of depth of burial than observed at Sites 897, 898, and 899. This difference is not apparent in the velocity measurements taken under pressure. One explanation of the data observed shipboard is that the sediments at Sites 897, 898, and 899 have a smaller compressibility coefficient than the more proximal sediments at Site 900. If so, sediments recovered from Site 900 would have undergone less rebound following recovery, resulting in the greater velocity vs. depth trend, which was observed at Site 900. Alternatively, pore pressure may be lower at Site 900 than at comparable depths at the other three sites, resulting in a higher effective pressure, more compaction during burial, and a higher in situ velocity gradient. The data from the shore-based experiments suggest that the former explanation is more likely. Apparently, the in situ velocities of sediments at all sites are comparable at similar depths. The higher velocity gradient measured aboard ship may thus be an artifact of differing amounts of decompaction following recovery, and it does not necessarily indicate different in situ velocity structure.

The estimated in situ velocity trend is in reasonable agreement with the velocity structure estimated from sonobuoy data (Whitmarsh et al., 1990), although the laboratory data appear to consistently exceed the seismically determined velocities (Fig. 6A). This may partially be a result of the constant velocity layer model determined from traveltime modeling of the seismic data, but it probably also reflects the large uncertainties involved in estimating the in situ effective pressure from the laboratory data. If the in situ effective pressure was systematically overestimated, the in situ velocities determined from the laboratory data would similarly be overestimated. The laboratory data are more consistent with the sonobuoy data if a linear increase in velocity is adopted in the upper acoustic layer (dotted line, Fig. 6A). A similar velocity gradient was observed in the shipboard velocity measurements in the upper 400 mbsf (Fig. 1). However, the sonobuoy data provide remarkably accurate estimates of the depth to major lithostratigraphic boundaries encountered during Leg 149. The in situ velocity structure must therefore not be greatly different than that interpreted by Whitmarsh et al. (1990) on the basis of the sonobuoy data, although traveltime modeling of the sonobuoy data does permit modest gradients in the velocity structure. Furthermore, the linear velocity gradient shown by the dotted line in Figure 6A does not result in a velocity discontinuity between acoustic Layers 1 and 2. The presence of a reflection in the sonobuoy data at the base of acoustic Layer 1 requires such a discontinuity (Whitmarsh et al., 1990). There is some evidence in the laboratory data for a rapid increase in velocity over a small depth interval, which may produce the reflection, although the laboratory data would place the change in velocity at a depth of about 335 to 370 mbsf, rather than 420 mbsf as indicated on the sonobuoy profile (Fig. 6A). This is not surprising, as the sonobuoy line and the various drill sites used in this study were distributed over a ~100 km distance. In this latter interpretation of the laboratory results (dashed line, Fig. 6A), acoustic Layer 1 is interpreted to show a modest increase in velocity to a depth of about 320 mbsf. A strong velocity gradient between the data points collected at 336

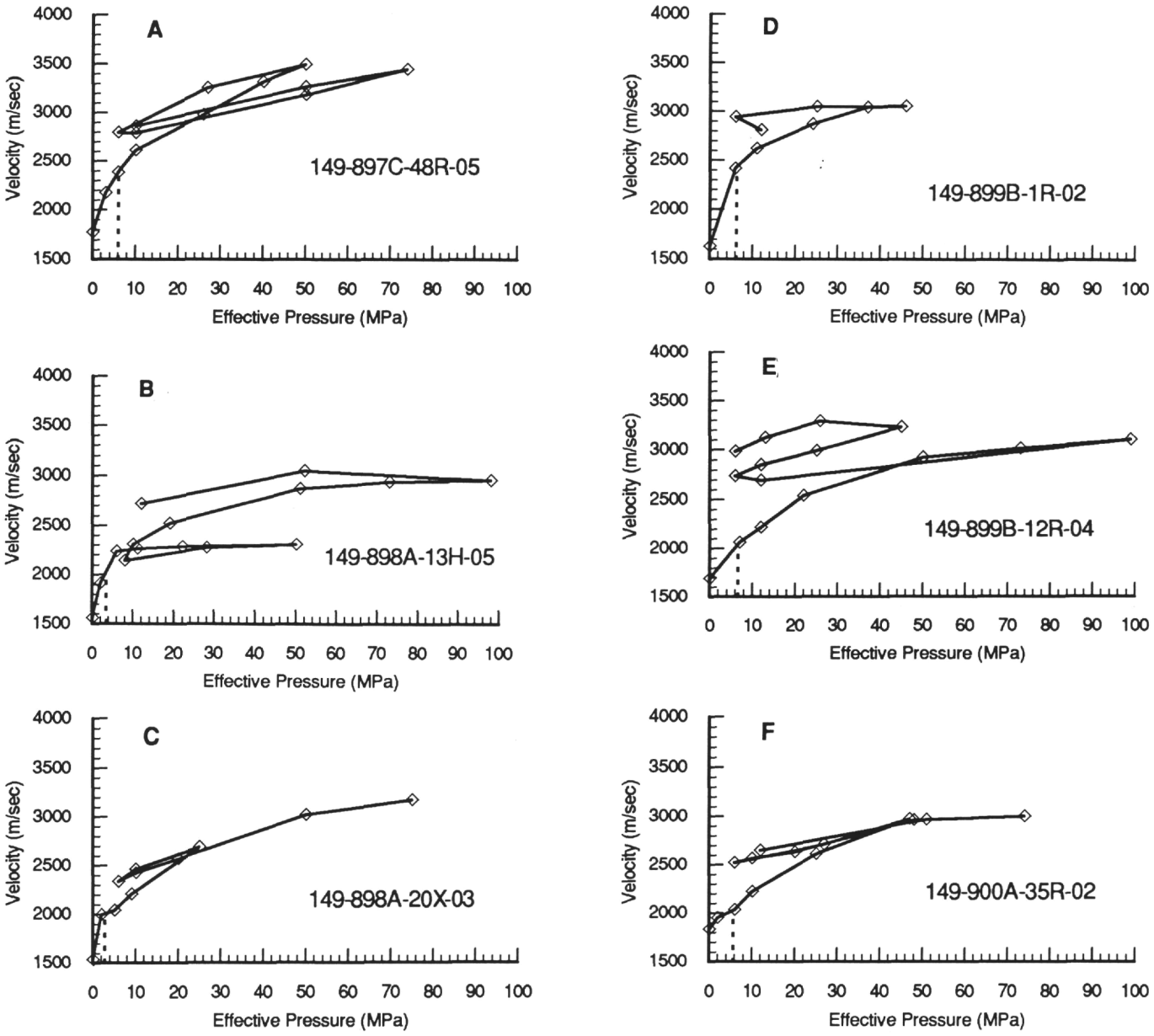

Figure 5. **A-F.** Corrected velocity curves for samples analyzed in this study. The vertical dashed line indicates the best estimate of the in situ effective pressure.

mbsf and 369 mbsf is interpreted to bound the layer that produces the reflection. This velocity gradient is somewhat apparent in the shipboard data (Fig. 1). The dashed line in Figure 6A is the preferred interpretation of the laboratory data. Nonvertically incident seismic rays will probably travel at velocities intermediate between the velocities given in the constant velocity model derived from the sonobuoy data and the linear velocity profile (derived from vertically incident data) shown by the dashed line in Figure 6A.

The second unanticipated aspect of the data shown in Figure 6 is the apparent increase in the in situ effective pressure from 2-3 MPa above about 200 mbsf to about 6 MPa below 200 mbsf. This is interpreted to indicate a transition from poorly consolidated sediments above 200 mbsf to consolidated sediments below 200 mbsf. Above 200 mbsf, grains are inferred to be in loose contact, allowing free pore-fluid migration. As a result, pore fluid is expelled with increasing depth of burial and effective pressure increases. Below 200 mbsf, grains are inferred to be in close contact and pore-fluid migration is restricted. Below this depth, the increase in confining pressure that results from the increasing depth of burial is largely balanced by an increase in pore-fluid pressure. As a result, effective pressure (and velocity) show little increase below this depth.

POROSITY AND DENSITY

Porosity is given by

$$\phi = V_w/(V_g+V_w), \quad (2)$$

where V_w is the volume of water contained in the sample and V_g is the volume of solid in the sample (Boyce, 1973). Porosity at atmospheric

pressure was measured in samples taken adjacent to those used in the shore-based study. The initial water and solid volumes are given by

$$V_w = V_0\phi_0 \tag{3}$$

$$V_g = V_0(1-\phi_0),$$

where Φ_0 is the porosity at atmospheric pressure measured shipboard and V_0 is the initial volume of the sample determined from caliper measurements of the sample dimensions prior to testing. Assuming the volume loss under pressure is due solely to a reduction in pore space, the porosity under pressure is given by

$$\phi(p) = (V_w+\varepsilon_v V_0)/(V_g+V_w+\varepsilon_v V_0), \tag{4}$$

where ε_v is the volumetric strain the sample undergoes during the pressure testing (the sign convention is that compression is negative). The in situ porosity is determine from Eq. 4 using the estimated in situ effective pressure. Assuming that strain is isotropic, the volumetric strain can be determined by linearly interpolating the sample shortening as discussed previously, applying an equal percentage of shortening in the vertical and horizontal dimensions. The estimated in situ porosity is plotted as a function of depth in Figure 7. The porosity is generally consistent with an exponential relationship similar to that used in other studies (e.g., Sclater and Christie, 1980):

$$\phi(z) = \phi_s e^{-cz}, \tag{5}$$

where Φ_s is the porosity at the seafloor. However, the large scatter in the data and the limited number of data points result in large variance in the fit. A least squares fit of Eq. 5 to the calculated in situ porosity yields c = 0.00064 m^{-1} and Φ_s = 0.52 with a correlation coefficient of 0.19. If Φ_s is assumed to be 1, the least squares fit gives c = 0.02957 m^{-1} with a correlation coefficient of 0.71. Curves showing both least-squares fits are shown in Figure 7.

By mass balance, density is given by

$$\rho(z) = \rho_g(1-\phi) + \rho_w\phi, \tag{6}$$

where ρ_g is the grain density (measured shipboard) and ρ_w is the density of seawater. The calculated in situ density is shown in Figure 8, and it can be reasonably described by a linear increase in density with depth:

$$\rho(z) = 1.7945 + 0.001\ z, \tag{7}$$

where density is in g/cm^3 and z is depth in meters.

SUMMARY

Comparison of shipboard acoustic velocity measurements from Leg 149 with velocities determined from seismic experiments shows that the shipboard data are poor indicators of in situ velocity in the sedimentary section beneath the Iberia Abyssal Plain. Experiments conducted under pressure yield estimated in situ velocities that agree well with seismic surveys on the Iberia Abyssal Plain. The laboratory data indicate a modest increase in velocity in the upper 335 mbsf, from about 1800 m s^{-1} at the seafloor to about 2000 m s^{-1} at 335 mbsf. A steep velocity gradient is interpreted in the interval between 335 and 370 mbsf, and it may be the cause of a reflection observed in the seismic data. An increase in effective pressure below about 200 mbsf is interpreted to represent a transition from poorly consolidated sediments to deeper consolidated sediments. Contrary to the shipboard acoustic velocity measurements, no evidence is seen for major differences in the velocity gradient in the upper 500 mbsf between Site 900 and Sites 897, 898, and 899. The steeper velocity gradient observed in the shipboard data from Site 900 is attributed to more pronounced decompression of the samples following recovery, which implies a difference between the geotechnical properties of the silty clays recovered at Site 900 and the other sites. The in situ porosity and density inferred from the laboratory experiments follow expected theoretical trends, indicating an exponential decrease in porosity and linear increase in density with depth.

Table 3. Estimated in situ effective pressure and velocity.

Core, section	P_e' (MPa)	Min/max	V_p (m/s)	Min/max
149-897C-				
34R-1	6.5	4.5/8.5	2250	2100/2400
48R-5	6.0	3.5/9.0	2380	2190/2510
149-898A-				
13H-5	3.7	2.0/5.5	2090	1912/2235
20X-3	2.2	0/5.0	1995	1530/2080
149-899B-				
1R-2	6.0	3.5/9.0	2470	2000/2600
12R-4	6.5	4.0/10.0	2075	1875/2120
149-900A-				
35R-2	5.6	2.0/10.0	2034	1951/2223

Notes: P_e' = effective pressure; V_p = estimated in situ P-wave velocity.

ACKNOWLEDGMENTS

We thank the Atlantic Richfield Company (ARCO) in Piano, Texas, and Kent Nielsen at the University of Texas at Dallas (UTD) for the use of their laboratories. We also thank Billy Smith for keeping the equipment running at both the ARCO and UTD labs. Leg 149 physical properties specialists Lotte Krawczyk, Juli Morgan, and Luis Pinheiro and laboratory technicians John Lloyd and Claudia Muller contributed greatly to collection and analysis of the shipboard data and formulation of the post-cruise research objectives. We thank Richard Carlson, Kent Nielsen, and Bob Whitmarsh for helpful reviews. This research was supported by USSSP grant 149-20761b to DLH.

REFERENCES

Boyce, R.E., 1973. Physical properties—methods. *In* Edgar, N.T., Saunders, J.B., et al., *Init. Repts. DSDP,* 15: Washington (U.S. Govt. Printing Office), 1115-1128.

Das, B.M., 1983. *Advanced Soil Mechanics:* New York (Hemisphere Publishing).

Hamilton, E.L., 1971. Prediction of in-situ acoustic and elastic properties of marine sediments. *Geophysics,* 36:266-284.

Lambe, T.D., and Whitman, R.V., 1969. *Soil Mechanics, SI Version:* New York (Wiley).

Sawyer, D.S., Whitmarsh, R.B., Klaus, A., et al., 1994. *Proc. ODP, Init. Repts.,* 149: College Station, TX (Ocean Drilling Program).

Sclater, J.G., and Christie, P.A.F., 1980. Continental stretching: an explanation of the post-mid-Cretaceous subsidence of the central north sea basin. *J. Geophys. Res.,* 85:3711-3739.

Stoll, R.D., 1977. Acoustic waves in ocean sediments. *Geophysics,* 42:715-725.

Tschebotarioff, G.P., 1952. *Soil Mechanics, Foundations, and Earth Structures:* New York (McGraw-Hill).

Whitmarsh, R.B., Miles, P.R., and Mauffret, A., 1990. The ocean-continent boundary off the western continental margin of Iberia, I. Crustal structure at 40°30'N. *Geophys. J. Int.,* 103:509-531.

Date of initial receipt: 1 December 1994
Date of acceptance: 22 May 1995
Ms 149SR-231

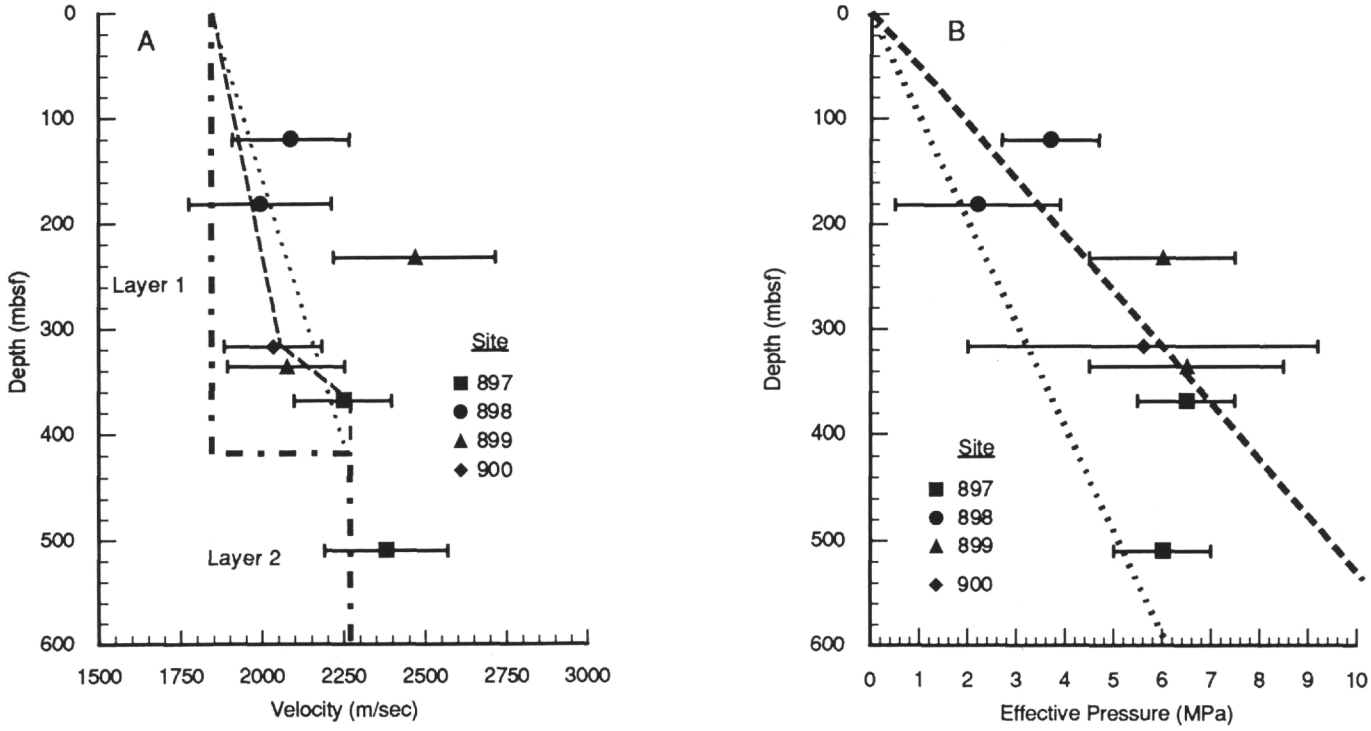

Figure 6. **A.** Estimated in situ velocity plotted as a function of depth of burial. The heavy dashed line is the velocity curve reported by Whitmarsh et al. (1990) for sonobuoy Line 1. Model 1 (dotted line) is a linear interpolation of the sonobuoy velocities between the seafloor and the top of acoustic Layer 2. Model 2 (dashed line) includes a moderate linear velocity gradient above 320 mbsf, and a steep velocity gradient between 320 and 370 mbsf. See text for discussion. **B.** Estimated in situ effective pressure plotted as a function of depth. Also shown are the hydrostatic pressure gradient (dotted line) and lithostatic pressure gradient (dashed line) assuming a constant density of 1.9 g/cm^3 (Sawyer, Whitmarsh, Klaus, et al., 1994).

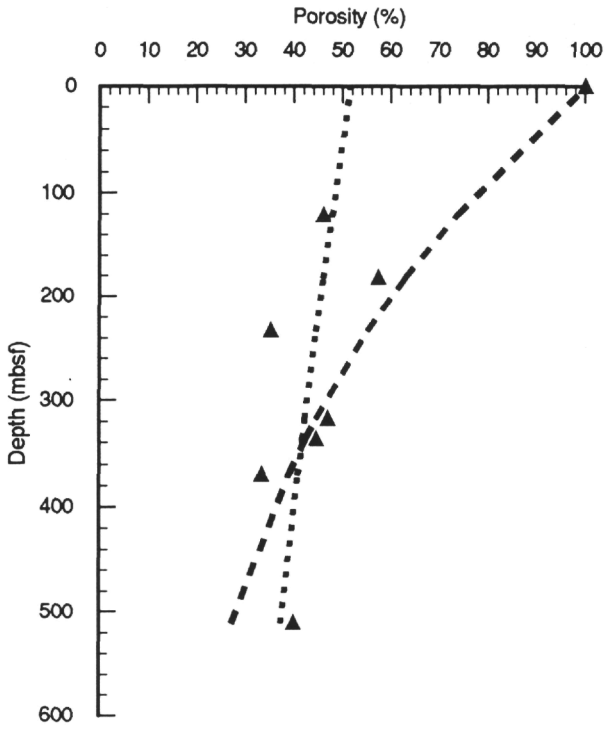

Figure 7. Estimated in situ porosity plotted as a function of depth of burial (triangles). The dashed line is the best-fit exponential trend, assuming porosity at the seafloor is 1. The dotted line is the best fit exponential curve based on no a-priori assumption of the porosity at the seafloor.

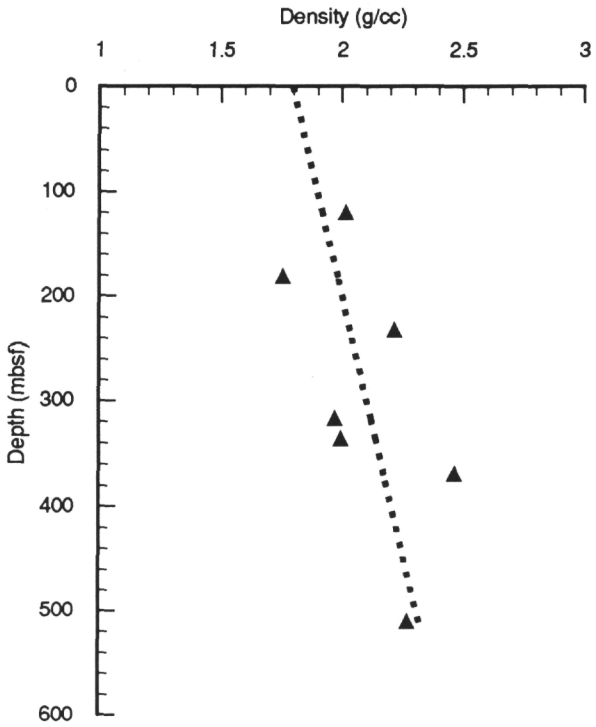

Figure 8. Estimated in situ density plotted as a function of depth (symbols). The best-fit linear trend is indicated by the dotted line.